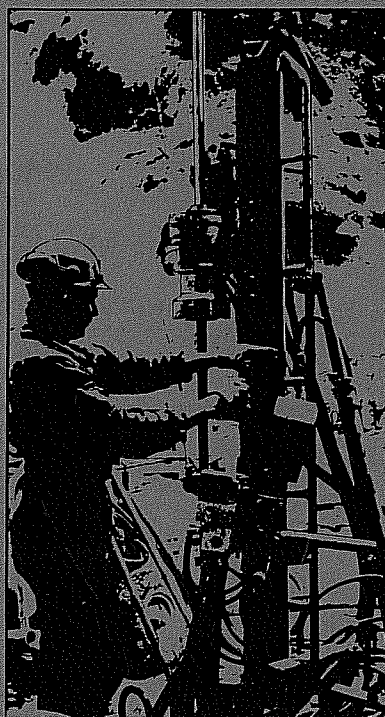


Andy D.  
LBL-7074  
SAC-03  
UC-70

SWEDISH-AMERICAN COOPERATIVE  
PROGRAM ON RADIOACTIVE WASTE STORAGE IN  
MINED CAVERNS IN CRYSTALLINE ROCK



Technical Project Report No. 3

THE MECHANICAL PROPERTIES  
OF STRIPA GRANITE

Graham Swan  
Division of Rock Mechanics  
University of Luleå  
Luleå, Sweden

August 1978

A Joint Project of

Swedish Nuclear Fuel Supply Co.  
Fack 10240 Stockholm, Sweden  
Operated for the Swedish  
Nuclear Power Utility Industry

Lawrence Berkeley Laboratory  
Earth Sciences Division  
University of California  
Berkeley, California 94720, USA  
Operated for the U.S. Department of  
Energy under Contract W-7405-ENG-48

This report was prepared as an account of work sponsored by the United States Government and/or the Swedish Nuclear Fuel Supply Company. Neither the United States nor the U.S. Department of Energy, nor the Swedish Nuclear Fuel Supply Company, nor any of their employees, nor any of their contractors, subcontractors, or their employees, makes any warranty, express or implied or assumes any legal liability or responsibility for the accuracy, completeness or usefulness of any information, apparatus, product or process disclosed, or represents that its use would not infringe privately owned rights.

Printed in the United States of America  
Available from  
National Technical Information Service  
U.S. Department of Commerce  
5285 Port Royal Road  
Springfield, VA 22161  
Price: \$4.50 Printed Copy

THE MECHANICAL PROPERTIES OF STRIPA GRANITE

Graham Swan

Division of Rock Mechanics  
University of Luleå  
Luleå, Sweden

Reprinted by Lawrence Berkeley Laboratory  
University of California  
Berkeley, California 94720

August 8, 1978

Originally part of KBS Teknisk Rapport 48, Kärnbränslesäkerhet (KBS)  
(Swedish Nuclear Fuel Safety Program)

September, 1977



## PREFACE

This report is one of a series documenting the results of the Swedish-American cooperative research program in which the cooperating scientists explore the geological, geophysical, hydrological, geochemical, and structural effects anticipated from the use of a large crystalline rock mass as a geologic repository for nuclear waste. This program has been sponsored by the Swedish Nuclear Power Utilities through the Swedish Nuclear Fuel Supply Company (SKBF), and the U.S. Department of Energy (DOE) through the Lawrence Berkeley Laboratory (LBL).

The principal investigators are L.B. Nilsson and O. Degerman for SKBF, and N.G.W. Cook, P.A. Witherspoon, and J.E. Gale for LBL. Other participants will appear as authors of subsequent reports.

Previously published technical reports are listed below.

1. *Swedish-American Cooperative Program on Radioactive Waste Storage in Mined Caverns* by P.A. Witherspoon and O. Degerman. (LBL-7049, SAC-01)
2. *Large Scale Permeability Test of the Granite in the Stripa Mine and Thermal Conductivity Test* by Lars Lundström and Håken Stille. (LBL-7052, SAC-02)



## TABLE OF CONTENTS

1. SUMMARY. . . . .	1
2. INTRODUCTION . . . . .	1
3. RESULTS. . . . .	3
3.1 Temperature dependency of Stripa granite. . . . .	3
3.1.1 Uniaxial compression tests. . . . .	4
3.1.2 Experimental determination of $\alpha_v$ . . . . .	9
3.1.3 Theoretical determination of $\alpha_v$ . . . . .	10
3.2 Triaxial compression tests. . . . .	12
3.3 "Brazilian" tensile fracture tests. . . . .	14
3.4 Laboratory shear box tests. . . . .	18
3.5 Anisotropy tests. . . . .	18
3.6 Dilatational wave velocity measurements . . . . .	21
4. DISCUSSION . . . . .	24
5. ACKNOWLEDGEMENTS . . . . .	24
6. REFERENCES . . . . .	24



## 1. SUMMARY

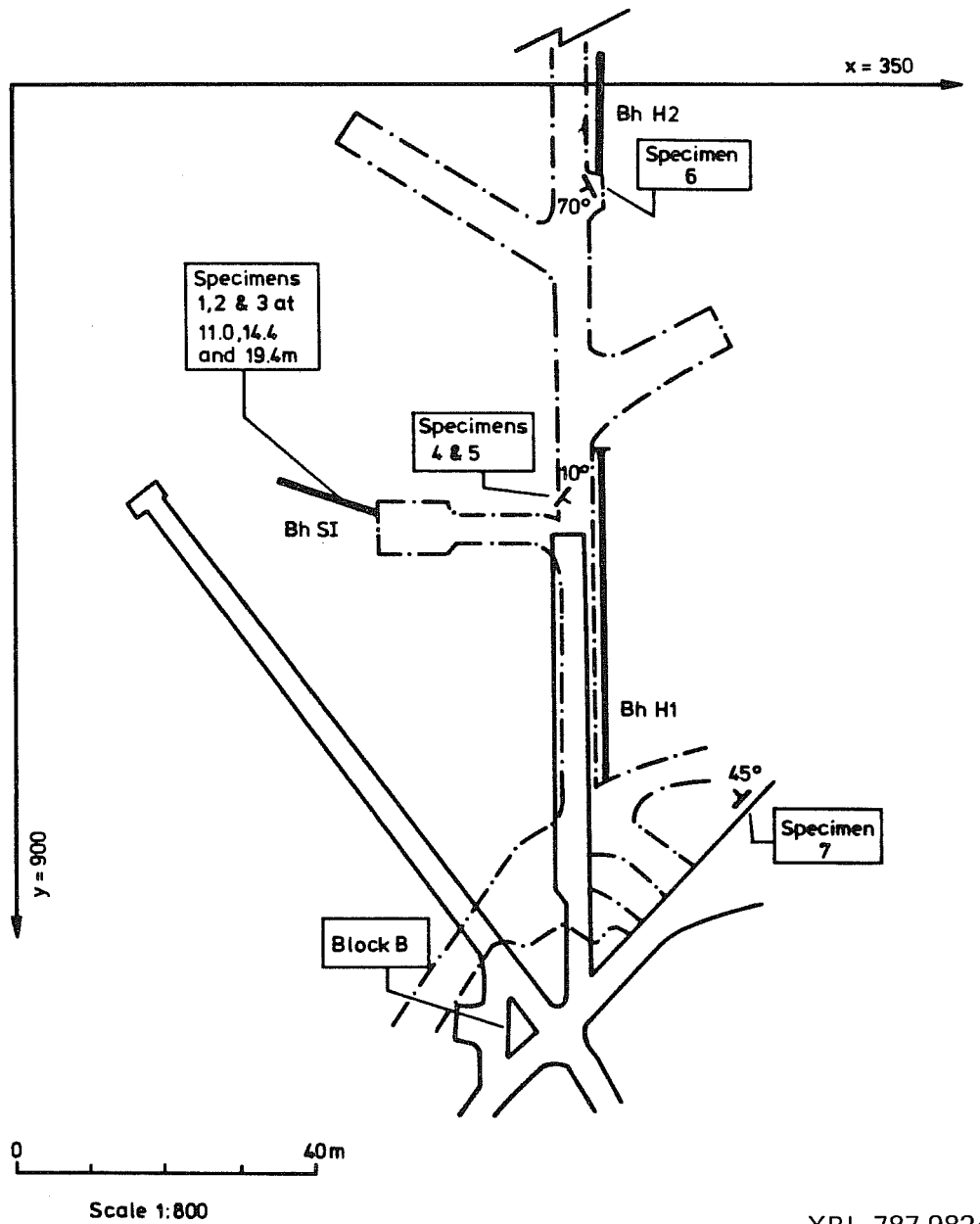
The mechanical properties of Stripa granite are presented as determined from small (laboratory size), oven-dried specimens. The properties determined include Young's modulus, Poisson's ratio, uniaxial compressive fracture stress, and the expansion coefficient, all as a function of temperature.

In addition the Brazilian tensile fracture stress, residual shear strength as a function of a normal stress and the rock's anisotropy ratios are presented. Finally ultrasonic determinations at 1 MHz of the rock's dilatational wave velocity are given and the deduced Young's modulus is compared with the static value for room temperature.

## 2. INTRODUCTION

For the determination of the mechanical properties of Stripa granite, samples were largely taken from the three boreholes DBH-1 (45 mm  $\phi$ ), DBH 2 (42 mm  $\phi$ ), and Bh V1 (45/42 mm  $\phi$ ). Additional samples were obtained from the 72 mm  $\phi$  borehole Bh SI, "hand specimens," and from the orientated block B (see Fig. 1). It was noticed that the granite type taken from these different sources is certainly of variable character. In an attempt to demonstrate this site variability, selection of the samples for each test was made at random, rather than systematically taking adjacent samples from a common borehole. As a useful guide to this variability, in the results given below a comparison is made wherever possible with Bohus granite, a fairly uniform, well-known Swedish rock.

For the purposes of the numerical calculations later to be performed



XBL 787-9824

Fig. 1. Map showing locations from which test specimens have been taken, P<sub>23</sub> Stripa.

in Object 10:03, it was decided that the following parameters should be determined:

- 3.1 Young's modulus ( $E$ , GPa)  
Poisson's ratio ( $\nu$ )  
Compressive fracture stress ( $\sigma_c$ , MPa)  
Expansion coefficient ( $\alpha$ ,  $\text{deg}^{-1}\text{C}$ )
- 3.2 Young's modulus ( $E$ , GPa)  
Compressive fracture stress ( $\sigma_c$ , MPa)
- 3.3 Brazilian tensile fracture stress ( $\sigma_T$ , MPa)
- 3.4 Residual shear stress ( $\tau_r$ , MPa) as a function of normal stress ( $0 < \sigma_n < 11$  MPa)
- 3.5 Anisotropy ratios for Young's modulus ( $E$ , GPa) and compressive fracture stress ( $\sigma_c$ , MPa)
- 3.6 Dilatational wave velocity ( $C_T$ , m/s) and deduced dynamic Young's modulus ( $E_{\text{dyn}}$ , GPa)

} as a function of temperature  
20 < t < 200°C

} as a function of confining pressure  
0 <  $\sigma_3$  < 30 MPa

Accompanying the results (3.1) through (3.6) given below, is a brief description of the test method used.

### 3. RESULTS

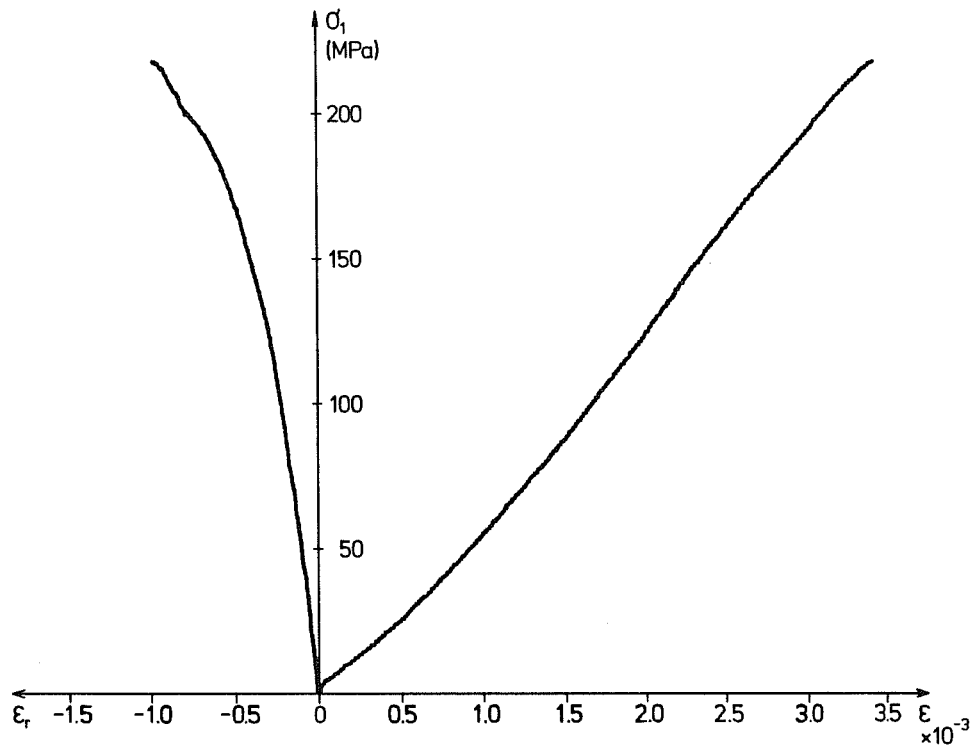
#### 3.1 Temperature Dependency of Stripa Granite

The results for this group are derived from (i) a series of uniaxial compression tests (obtaining  $E$ ,  $\nu$  and  $\sigma_c$  as functions of temperature) and (ii) a theoretical calculation based on Simmons' work [1] and experiments also developed by Simmons, which make use of a differential dilatometer [2] (obtaining the coefficient of cubical expansion  $\alpha_v$  as a

function of temperature).

3.1.1 Uniaxial Compression Tests. The specimens prepared for this test were 45 mm diameter cores cut to a length of 105 mm and oven dried at 80°C for 2 days. All strain measurements were made using strain gauges (type HBM 61 120 LY11, 20° < T < 150°C and type HBM 61 120 LG11, T > 150°C) glued to the specimens. Each specimen was then lined with a thin plastic protection and heated for 2-3 hours in an oven to the pre-determined equilibrium temperature. It was then placed into a heated oil bath and loaded to failure in a conventional uniaxial compression test. At temperatures over 100°C precautions were taken to eliminate gross heat losses from the oil bath via conduction and convection. Even so, because of the limitations of the method, it was only possible to maintain the high testing temperatures to within about ±5% of the pre-determined value.

From each test a plot of axial stress  $\sigma_1$  against axial strain  $\epsilon_1$  and radial strain  $\epsilon_r$  was obtained, an example of which is shown in Fig. 2. The values of E,  $\nu$  and  $\sigma_c$  derived from such a plot are given comprehensively in Table I. It should be noted that both E and  $\nu$  are evaluated from secants drawn from the origin to intersect the curves at  $\sigma_1 = 50\% \sigma_c$ . A statistical summary of these results is given in Table II. Also appearing in Table II are the comparative data at room temperature for Bohus granite. The two rock types may also be compared in Plate I which shows the typical post-failure fracture surfaces resulting from the test. Graphical presentations of Table II are given in Figs. 3 and 4.



XBL 787-9825

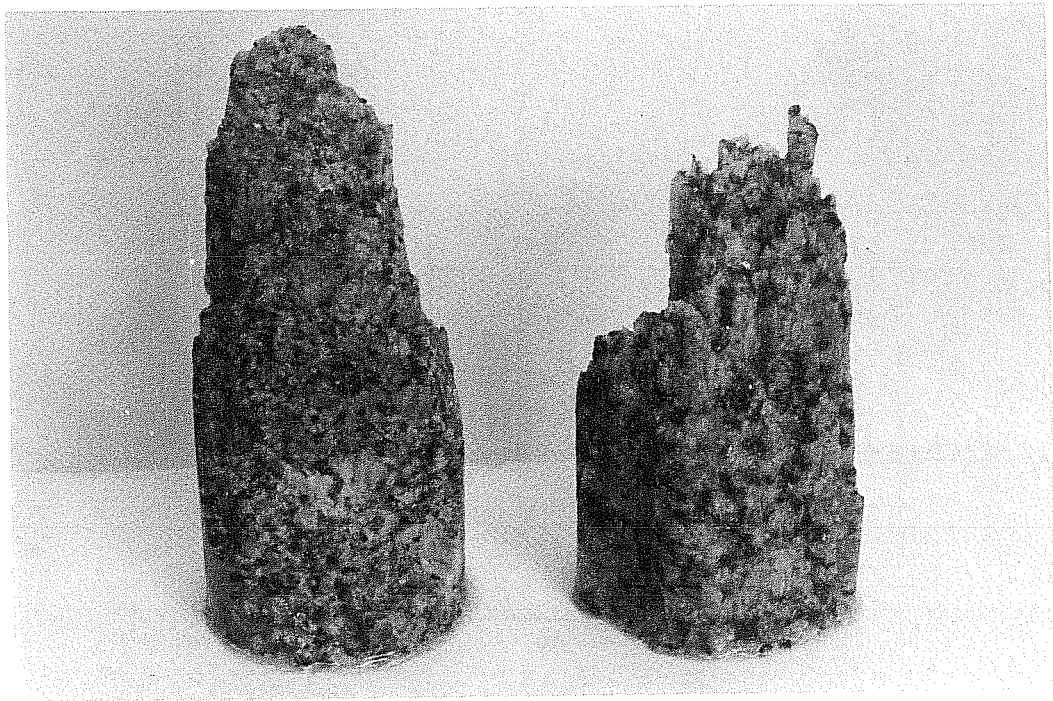
Fig. 2. Typical stress vs. strain plot from uniaxial test at 150°C [Specimen E22].

TABLE I. Comprehensive results from uniaxial compression tests.

Oil bath temp. °C	Specimen number	Fracture stress $\sigma_c$ MPa	Young's Modulus E GPa	Poisson's ratio $\nu$	Failure Description (see footnote)
20	V1 43.57 E1	192.0	72.4	0.27	1
20	H1 33.30 E3	207.7	63.0	-	1
20	V1 44.25 E5	229.9	67.4	0.23	2
20	H1 30.10 E6	217.9	61.8	0.15	2
20	V1 39.80 E7	180.9	78.4	0.23	1
20	H1 29.25 E8	247.9	68.0	0.19	1
20	H1 35.65 E9	222.0	64.0	0.20	1
20	V1 44.70 E10	149.0	68.8	0.19	3
20	H1 29.45 E11	245.6	67.8	0.20	1
20	H1 28.60 E12	182.8	82.0	0.22	1
51-49	V1 42.00 E31	177.8	70.2	0.18	2
50	V1 52.36 E32	192.9	68.6	0.29	1
50	H1 28.30 E33	200.6	67.4	0.23	1
50	V1 44.35 E34	259.2	80.0	0.27	1
50	V1 45.02 E35	228.7	67.6	0.19	1
50	H1 29.35 E36	187.3	68.4	0.15	2
50	H1 28.40 E37	231.4	73.4	0.20	1
50	V1 44.60 E38	187.6	73.4	0.19	3
105-73	H1 24.00 E13	218.6	60.8	0.27	1
120-110	H1 13.40 E14	249.0	57.8	-	1
100-92	V1 39.31 E15	219.9	61.0	0.22	1
101-94	V1 43.30 E16	213.1	62.6	0.22	2
101-96	H1 14.45 E17	190.7	67.4	0.19	3
104-99	H1 7.63 E18	228.7	61.6	0.18	1
102-97	H1 16.35 E19	229.1	66.2	0.11	1
152-140	H1 19.80 E20	208.2	60.6	0.17	2
155-151	H1 16.45 E21	178.0	51.2	0.11	3
155-147	H1 23.75 E22	217.6	60.0	0.13	1
155-148	V1 39.21 E24	231.1	55.8	0.26	1
158-148	H1 41.50 E25	212.0	53.6	0.15	1
157-150	H1 31.80 E26	186.1	61.8	0.12	2
188-170	H1 28.75 E29	194.9	47.6	0.20	2
197-175	V1 44.12 E30	129.6	53.0	-	2
194-170	V1 44.02 E39	143.1	49.6	0.09	2
197-180	H1 29.62 E40	114.3	58.4	0.12	2
195-191	V1 38.02 E41	155.9	44.6	0.14	2
195-180	V1 38.12 E42	150.1	51.0	0.10	2

Note:

- 1 Complete failure
- 2 Partial failure: edge spall
- 3 Partial failure: weakness plane



XBB 788-9385

Plate 1. Appearance of failed specimens after uniaxial compression test, Bohus granite left, Stripa granite right.

TABLE II. Statistical summary of Table I.

Sample Size	Mean Temp °C	Fracture Stress $\sigma_c$ MPa		Young's Modulus E GPa			Poisson's Ratio $\nu$		
		mean	standard dev.	mean	standard dev.	90 % conf. lmts.	mean	standard dev.	90 % conf. lmts.
10	20	207.6	31.4	69.4	6.6	73.4 65.4	0.21	0.03	0.191 0.229
8	50	208.2	28.4	71.2	4.4	74.2 68.2	0.21	0.05	0.175 0.245
7	100	221.3	17.8	62.4	3.4	65.0 59.8	0.20	0.05	0.159 0.241
6	150	205.5	19.9	57.2	4.2	60.8 53.6	0.16	0.06	0.111 0.209
6	190	148.0	27.4	50.8	4.8	54.8 46.8	0.13	0.04	0.091 0.169
Bohus Granite (Room temp)		157.0	43.0	53.3	2.6	-	0.20	0.01	-

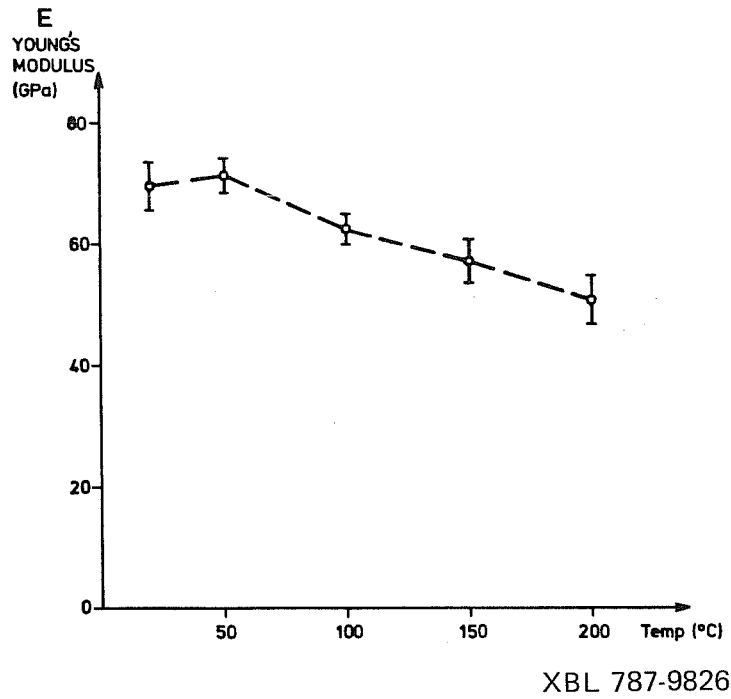


Fig. 3. Young's modulus vs. temperature, showing 90% confidence limits.

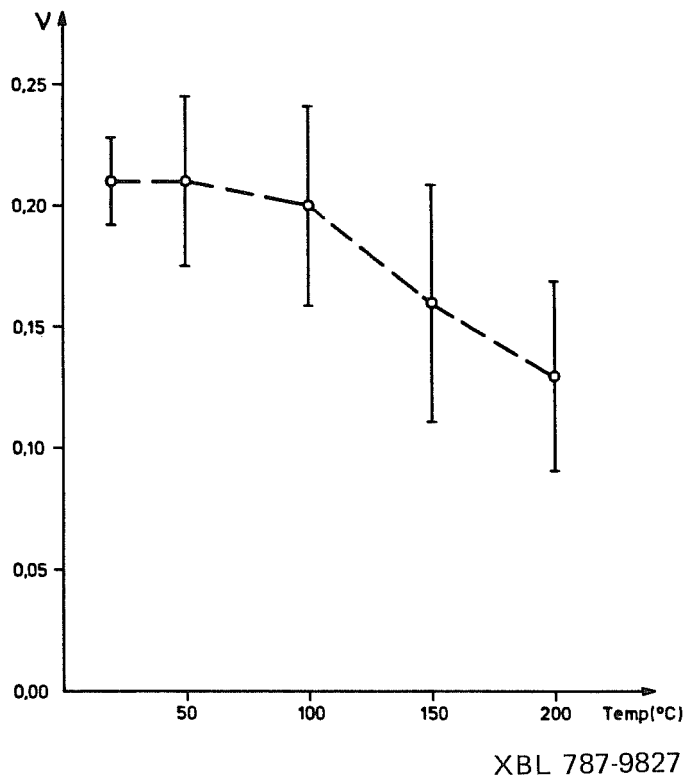
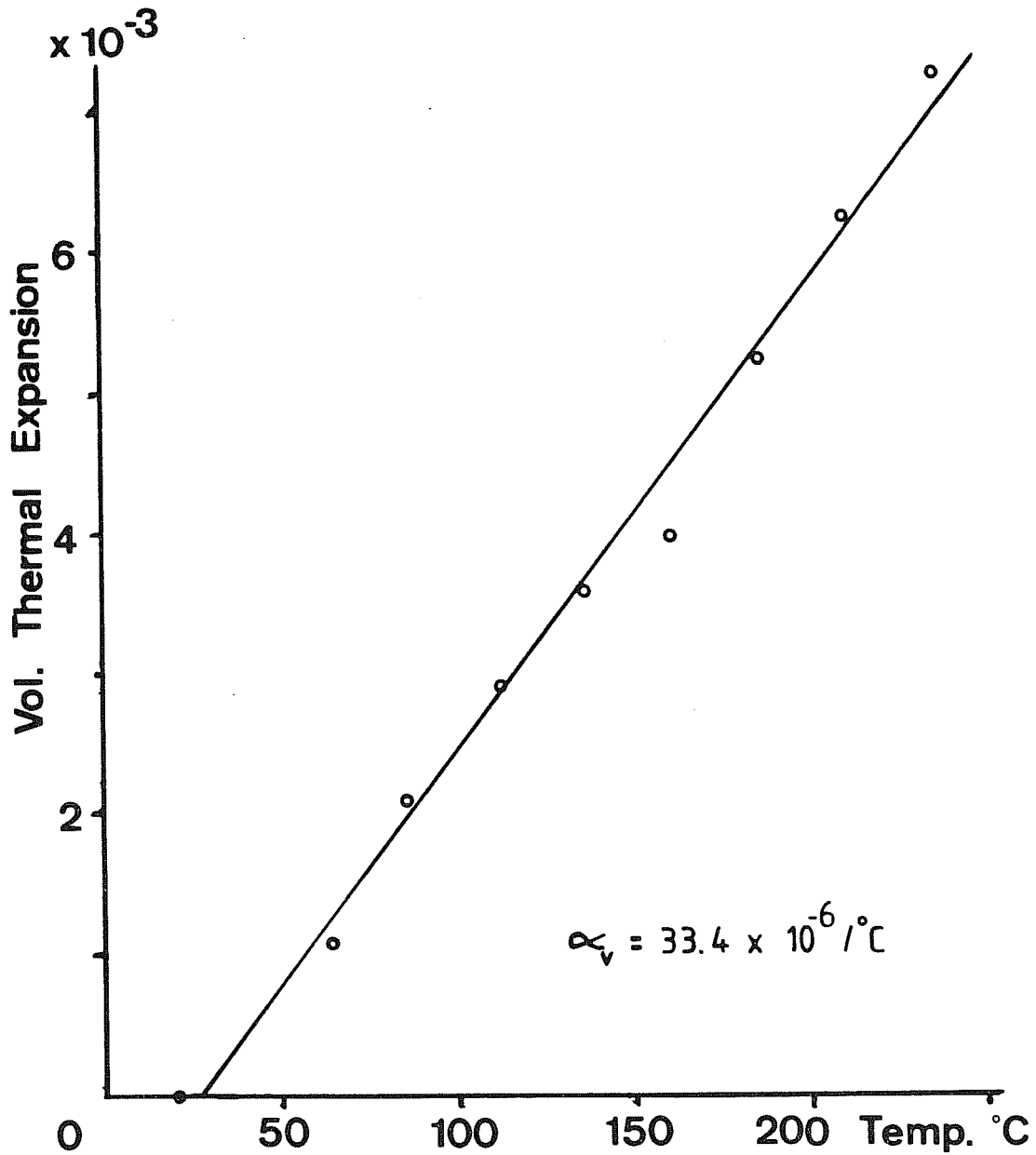


Fig. 4. Poisson ratio vs. temperature, showing 90% confidence limits.

3.1.2. Experimental Determination of  $\alpha_v$  as a Function of Temperature.

The preliminary results\* from  $\alpha_v$  determinations on the Stripa granite are presented below in Table IV/V and in Fig. 5/6. For the purpose of theoretically calculating  $\alpha_v$  (see section 3.1.3) and for



XBL 787-9828

Fig. 5/6. Volumetric thermal expansion vs. temperature.

\*Supplied by Terra Tek and based on one sample only.

general reference, the modal composition of the light-red granite variety is given in Table III.

### 3.1.3 Theoretical Determination of $\alpha_v$ as a Function of Temperature.

It has been shown by Cooper and Simmons [1] that  $\alpha_v$  may be calculated theoretically for a number of different rock types and agreement with measured values, for the most part, is reasonably good. They obtained their theoretical  $\alpha_v$  values using the composite expression:

$$\alpha_v = \frac{\sum \alpha_i E_i V_i}{\sum E_i V_i}$$

where  $\alpha_i$  = coefficient of cubical expansion of  $i^{\text{th}}$  phase  
 $E_i$  = Young's modulus of  $i^{\text{th}}$  phase  
 $V_i$  = volume fraction of  $i^{\text{th}}$  phase

Table III gives the value of  $V_i$  for the 5 phases occurring in

TABLE III. Modal composition of Stripa granite.

Mineral	Volume %
Quartz	43.6
Potash felspar	12.0
Plagioclase felspar	39.2
Muscovite	2.0
Chlorite	3.2
Total	100.0
Number of points	1 396

Stripa granite. From the two available reference books [3] and [4] it is possible to extract data for  $E_i$  and  $\alpha_i$  for different minerals commonly found in granites (see Table VI).

TABLE IV/V. Preliminary results (based on one sample only) from  $\alpha_v$  determination.

Temperature $^{\circ}\text{C}$	Vol. expansion $\times 10^{-3}$
21	0.000
65	1.074
86	2.106
113	2.913
137	3.606
161	3.978
186	5.211
211	6.252
237	7.263

TABLE VI. Data used for calculation of  $\alpha_v$ .

Mineral	$\alpha$ ( $25^{\circ}\text{C}$ )	$\alpha$ ( $400^{\circ}\text{C}$ )	E (GPa)
Quartz	34	69	95.7
K-felspar	15	20	73.9
Plagioclase	13	17	88.1
Muscovite	(20)	(25)	78.8
Biotite	(20)	(25)	68.3
Opagues	29	45	230.5

These data have been used for the calculation of  $\alpha_v$  both at 25°C and at 400°C for a number of granite types, including Stripa granite, Table VII. Included in this table are the comparative experimental and theoretical values given by Cooper and Simmons [1]. The reason for the discrepancy in the independently calculated theoretical values remains, as yet, to be explained.

### 3.2 Triaxial Compression Tests

Specimens for the triaxial compression tests were taken from bore-hole H2, cut to lengths of 84 mm, and oven dried at 80°C for two days. Each specimen was then sealed in an impervious rubber jacket and placed in turn into a conventional triaxial cell. An electric oil pump with drain valves then maintained the equal minor principal stress level

TABLE VII. Comparison between measured and calculated coefficients of thermal expansion.

Rock type	Specimen No	$\alpha_v(25^{\circ}\text{C}) \times 10^{-6}$			$\alpha_v(400^{\circ}\text{C}) \times 10^{-6}$		
		Experiment Ref. [1]	Theory Ref. [1]	Theory, Present work	Experiment Ref. [1]	Theory Ref. [1]	Theory, Present work
Stripa granite	-	-	26.6	23.4	-	44.2	41.9
Chelmsford granite	A757	21.5	25.3	21.2	73.3	37.5	36.3
Westerly granite	1134	24.8	22.6	19.6	67.0	32.9	32.1
Wausau granite	1343	19.9	27.2	23.4	71.5	41.0	41.8
Graniteville granite	1410	25.1	25.5	21.5	76.8	38.1	37.4
Red River Quartzmon.	1370	21.2	25.0	21.0	75.0	37.0	35.5

constant, while the axial load was increased in a 300 Ton machine to the specimen's failure load. This load was noted for increasing values of confining pressure  $0 < \sigma_3 = \sigma_2 < 30$  MPa.

The comprehensive data from these tests are given in Table VIII and the statistical summary is in Table IX. A plot of axial stress  $\sigma_1$  against axial strain  $\epsilon_1$  for different confining pressures as obtained

TABLE VIII. Comprehensive results from triaxial compression tests.

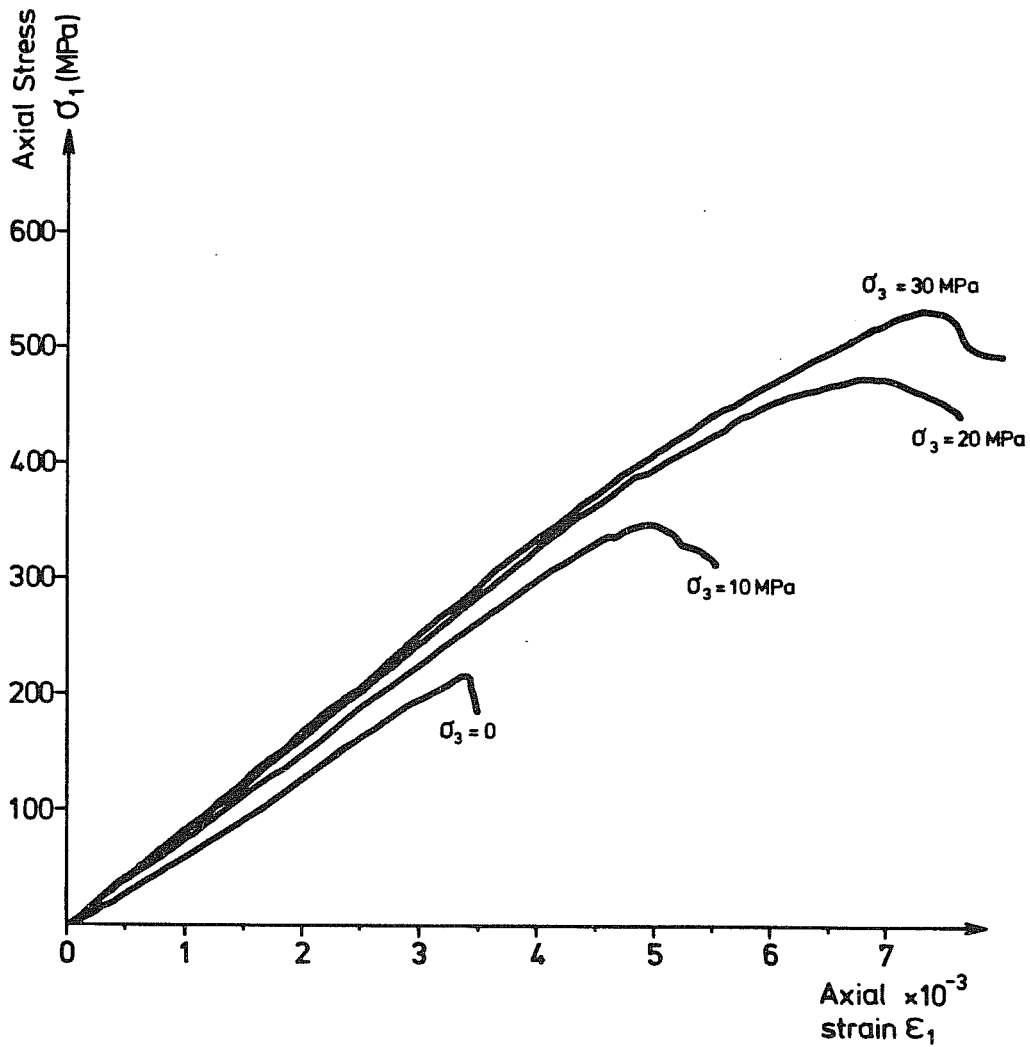
Confining Pressure $\sigma_3 = \sigma_2$ (MPa)	Specimen Number	Fracture Stress $\sigma_c$ (MPa)	Young's Modulus E (GPa)	Failure Description (see footnote)
5	H2 9.70 T22	302	75.4	1
5	H2 51.35 T23	317	72.2	1
5	H2 86.70 T24	319	75.6	1
5	H2 84.25 T25	296	77.6	1
5	H2 3.50 T26	266	76.2	2
10	H2 85.6 T7	352	76.8	1
10	H2 5.50 T8	408	78.6	1
10	H2 5.50 T10	384	77.4	1
10	H2 42.15 T11	344	76.2	1
20	H2 17.30 T12	476	83.0	1
20	H2 5.90 T13	478	84.8	1
20	H2 5.70 T14	462	83.8	1
20	H2 73.20 T15	470	78.8	1
20	H2 15.75 T16	464	80.6	1
30	H2 9.90 T17	516	82.6	1
30	H2 9.80 T18	480	82.8	2
30	H2 15.65 T19	533	83.2	1
30	H2 87.00 T20	520	83.2	1
30	H2 15.90 T21	552	84.2	1

Note: 1 Complete failure  
2 Failed on weakness plane

from the tests is shown in Fig. 7. The data of Table IX is also plotted, as seen in Fig. 8. A typical barrel-shaped failed specimen is shown in Plate 2.

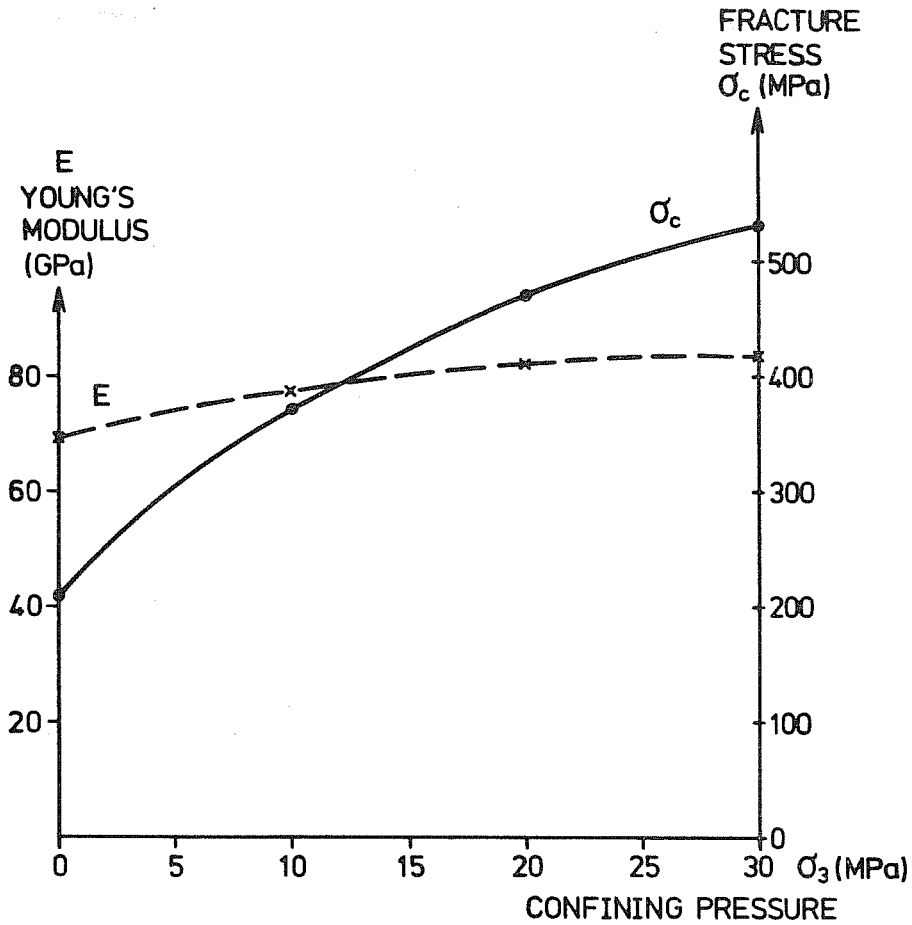
### 3.3 "Brazilian" Tensile Fracture Tests

The specimens used in this test were taken from 72 mm diameter cores cut to lengths of 36 mm, and oven dried for 2 days at 80°C. It only remained to compress each specimen under diametrically opposite



XBL 787-9829

Fig. 7. Axial stress vs. strain plots for confining pressures  $\sigma_2 = \sigma_3$  of 0, 10, 20 and 30 MPa.



XBL 787-9830

Fig. 8. Graph showing the variation of Young's modulus and fracture stress  $\sigma_c$  with confining pressure.

TABLE IX. Statistical summary of Table VIII.

Confining Pressure (MPa)	Fracture stress $\sigma_c$ (MPa)		Young's Modulus E (GPa)	
	mean	standard deviation	mean	standard deviation
5	308.5	9.8	75.4	1.78
10	372.0	25.6	77.2	0.88
20	470.0	6.3	82.2	2.20
30	530.3	14.0	83.2	0.56

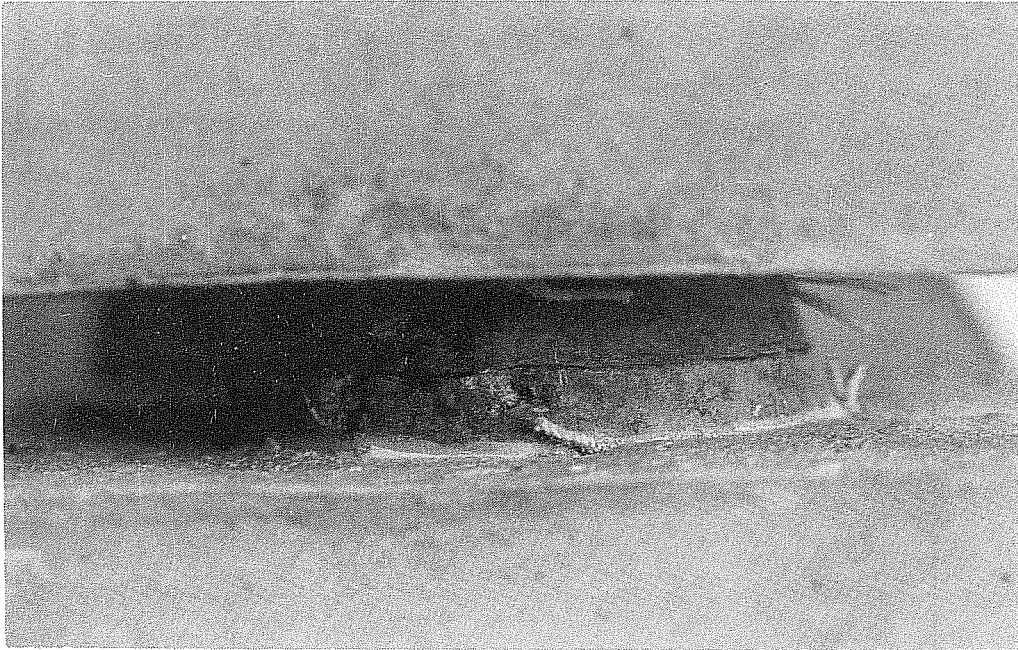


Plate 2 A. A jointed specimen shown encapsulated in concrete.



XBB 788-9387

Plate 2 B. Appearance of a natural joint surface. The dark features are due to the presence of chlorite.

loads and to note the failure load P. Ideally P should be the point failure load, but in practice local crushing occurs and so P is actually applied over a small angle  $2\alpha$ . The value of this angle was estimated to be  $4.8^\circ$ , from which the tensile failure stress was calculated using  $\sigma_T = -2.45 \times 10^2 P$ . The complete data from these tests are shown in Table X, as well as the statistical summary and the comparative values

TABLE X. Complete results from "Brazilian" tensile fracture tests.

Specimen number	Failure Load P	Tensile fracture stress $\sigma_T$
	kN	MPa
B1 SI 4.41	61.2	14.99
B2 SI 4.41	63.9	15.66
B3 SI 1.55	67.5	16.54
B4 SI 9.08	65.7	16.10
B5 SI 9.08	56.7	13.89
B6 SI 1.55	76.5	18.74
B7 SI 9.60	60.3	14.77
B8 SI 1.55	67.5	16.54
B11 SI 9.08	51.3	12.57
B15 SI 9.60	54.0	13.23
B16 SI 6.53	54.0	13.23
B17 SI 6.53	54.0	13.23

	"Brazilian" fracture stress $\sigma_T$		
	mean MPa	standard deviation	90 % Conf. limits
Stripa granite	14.96	1.75	13.9 15.9
Bohus granite	10.50	0.63	-

for Bohus granite.

### 3.4 Laboratory Shear Box Tests

Specimens for this test were selected from 72 mm diameter cores and from hand specimens (see Fig. 1 for locations) all having natural joint surfaces. Each specimen was first oven dried and then encapsulated in a concrete mould (see Plate 3). The equipment used for the test was a standard Robertson's field shear box. A general description of each joint surface tested is given in Table XI. The dominating fill material in all cases was chlorite. A plot showing the dependency of residual shear strength ( $\tau_r$ ) on joint normal pressure ( $\sigma_n$ ,  $0 < \sigma_n < 11$  MPa) is shown in Fig. 9. It is apparent from this figure that the residual shear strength may be described by the bilinear relationships:

$$\sigma_r = \sigma_n \tan \phi_{r1}, \quad 0 < \sigma_n < 3.4 \text{ MPa}$$

where  $\phi_{r1} = 32.7^\circ$

and

$$\sigma_r = \sigma_n \tan \phi_{r2} + S_0, \quad 3.4 < \sigma_n < 11 \text{ MPa}$$

where  $\phi_{r2} = 24.8^\circ$  and  $S_0 = 0.71 \text{ MPa}$

The upper limit of 11 MPa in the second equation is fixed by the strength of the encapsulating material (concrete) of the test, and by the joint area of the specimen. Predictions made outside the above stated limits should be treated cautiously.

### 3.5 Anisotropy Tests

In order to measure the anisotropy in a material like granite it is necessary to take extensive samples from a coordinated block in the



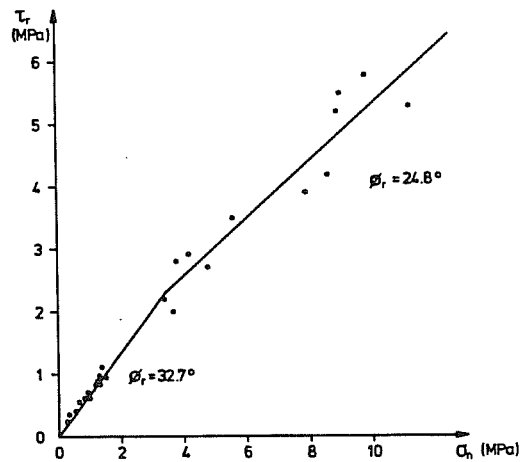
XBB 788-9386

Plate 3. Appearance of failed specimen after triaxial compression test,  $\sigma_3 = \sigma_2 = 20$  MPa. The rubber surround has been cut away after the test.

TABLE XI. General description of joints tested.

Specimen number	Joint surface Area (cm <sup>2</sup> )	Joint fill thickness (mm)	Surface structure (see footnote)
1	44.60	1-3	1
2	44.50	0-1	3
3	40.80	0-1	2
4	46.35	1-3	1
5	31.10	1-3	2
6	39.20	0.5-1	2
7	35.60	1-2	2

- Notes:
1. Dominantly plane
  2. Plane with rough irregularities
  3. Plane with marked roughness



XBL 787-9831

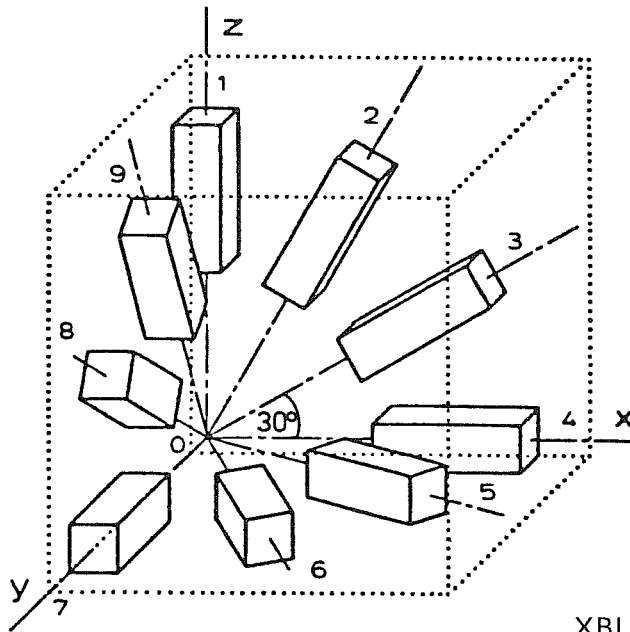
Fig. 9. Residual shear strength  $\tau_r$  as a function of normal joint pressure  $\sigma_n$ .

manner shown, Fig. 10. For this purpose a block with known orientation was taken from the Stripa mine and from this block it was proposed to recover 5 core specimens 42 mm  $\phi$  x 84 mm length from each angled hole. Unfortunately, owing to the jointed state of the block, core recovery was poor. It was therefore decided that instead of completing the full-scale anisotropy tests as planned, a small-scale test in one plane (x-z plane) would serve as an indication of anisotropy. The variables in which anisotropy should be observed were taken to be Young's modulus, compressive fracture stress, and dilatational wave velocity.

The complete results from these tests are given in Table XII. The sample size of 2 for each angle is not of course acceptable for a definitive statement on anisotropic behavior. However a trend is apparent in the sampled x-z plane with regard to both Young's modulus and dilatational wave velocity.

### 3.6 Dilatational Wave Velocity Measurements

Dilatational wave velocities ( $C_1$ ) were measured in oven-dried cylindrical specimens cut to lengths of 105 mm. Travel times were determined over this path length by an ultrasonic pulse technique at 1 MHz. The data obtained in this way together with the measured specimen densities are shown in Table XIII. Knowing the unconfined Young's modulus and Poisson's ratio (see Table III) it is possible to calculate a theoretical value for  $C_1$ . This value is also given in Table XIII where it is seen to be approximately 5% higher than the observed value of 5213 m/s. Alternatively, knowing  $C_1$  experimentally and assuming  $v_{\text{dynamic}} = v_{\text{static}}$ , a dynamic value for Young's modulus  $E_{\text{dyn}}$  may be estimated to have a value  $\approx$  63.3 GPa. However, in order to obtain  $E_{\text{dyn}}$



XBL 787-9832

Fig. 10. Sampling configuration for full-scale anisotropy test.  
(Test samples are cylinders.)

TABLE XII. Small-scale anisotropy test results.

Specimen number	Density (kg/m <sup>3</sup> )	C <sub>1</sub> Wave velocity		E Young's Modulus		$\sigma_c$ (MPa)
		(m/s)	mean s.d.	(GPa)	mean s.d.	
B1.1	2616.9	5164.2	5180.3	66.8	64.9	227.4
B1.2	2616.9	5196.3	±16.1	63.0	±2.0	81.2
B2.1	2614.4	5268.8	5240.9	65.8	65.2	237.2
B2.2	2609.8	5213.0	±27.9	64.6	±0.6	227.4
B3.1	2613.8	5310.1	5311.1	64.4	65.5	207.6
B3.2	2616.3	5312.1	±1.0	66.6	±1.2	233.9
B4.1	2617.8	5353.5	5381.6	64.4	65.7	181.2
B4.2	2619.7	5409.7	±28.1	67.0	±1.4	234.8

TABLE XIII. Density and dilatational wave velocity data and results.

Specimen number	Density $\rho$ (kg/m <sup>3</sup> )	Dilatational Wave velocity $C_1$ (m/s)
H2 6.60	2619	5123
H2 10.02	2630	5117
H2 10.13	2622	5132
H2 14.87	2625	5266
H2 30.57	2616	5230
H2 31.04	2521	5261
H2 31.15	2625	5255
H2 64.19	2627	5187
H2 77.23	2617	5296
mean	2622.5	5213.8
standard deviation	4.2	64.8
Calculated dilatational wave velocity $C_1 = [E(1-\nu)/(1+\nu)(1-2\nu)\rho]^{1/2}$		5457.9

more precisely it is necessary to measure the distortional wave velocity, but this has not been done in the present work.

#### 4. DISCUSSION

The Stripa granite as taken from the site locations of Fig. 1 is a relatively coarse-grained material which on the scale of laboratory testing strongly exhibits linearly elastic behavior. In comparison with other granites both its Young's modulus and its compressive fracture stress are high. This is likely to be accounted for by its high quartz content. The temperature dependency of its elastic properties within the range  $25 < T^{\circ}\text{C} < 200$  is similar to that of a granite reported elsewhere [5]. The large-scale properties of Stripa granite will to a great extent be determined by its strongly jointed (fractured) nature. This may be inferred with even greater certainty where chlorite-filled joints exist as a result of retrograde metamorphism.

#### 5. ACKNOWLEDGMENT

The assistance of Thomas Olofsson and Kenneth Mäki in the preparing and testing of rock specimens is gratefully acknowledged. Thanks is also due to Ove Alm for help and advice in the triaxial testing and to those at M.I.T., Department of Earth and Planetary Sciences, who kindly supplied experimental data for the thermal expansion of the rock.

#### 6. REFERENCES

- [1] The effect of cracks on the thermal expansion of rocks, Cooper, H.W. and Simmons, G., Earth and Planetary Sc. Letters, 1977 (in press).

- [2] Thermal expansion behavior of Igneous rocks, Richter, D. and Simmons, G., Int. Jnl. Rock Mech. Min. Sc., Vol. 11, pp. 403-411, 1974.
- [3] Thermal Expansion, Skinner, B.J., in Handbook of Physical Constants, G.S.A. Memoir 97, p. 75, 1966.
- [4] Single Crystal Elastic Constants and Calculated Aggregate Properties, Simmons G. and Wang H., M.I.T. press, Cambridge, 1971.
- [5] Thermal Guidelines for a Repository in Bedrock, Published Report of Parsons, Brinckerhoff, Quade & Douglas, Inc., New York, 1976.



This report is part of a cooperative Swedish-American project supported by the U.S. Department of Energy and/or the Swedish Nuclear Fuel Supply Company. Any conclusions or opinions expressed in this report represent solely those of the author(s) and not necessarily those of The Regents of the University of California, the Lawrence Berkeley Laboratory, the Department of Energy, or the Swedish Nuclear Fuel Supply Company.

Reference to a company or product name does not imply approval or recommendation of the product by the University of California or the U.S. Department of Energy to the exclusion of others that may be suitable.

TECHNICAL INFORMATION DEPARTMENT  
LAWRENCE BERKELEY LABORATORY  
UNIVERSITY OF CALIFORNIA  
BERKELEY, CALIFORNIA 94720

